Pressure-induced topological phase transitions and strongly anisotropic magnetoresistance in bulk black phosphorus

Chun-Hong Li,[1] Yu-Jia Long,[1] Ling-Xiao Zhao,[1] Lei Shan,[1,2] Zhi-An Ren,[1] Jian-Zhou Zhao,[1,3] Hong-Ming Weng,[1,2] Xi Dai,[1,2] Zhong Fang,[1,2] Cong Ren,[1,4,*] and Gen-Fu Chen[1,2,†]

[1]*Beijing National Laboratory for Condensed Matter Physics, Institute of Physics, Chinese Academy of Sciences, P.O. Box 603, Beijing 100190, China*

[2]*Collaborative Innovation Center of Quantum Matters, Beijing 100190, China*

[3]*Co-Innovation Center for New Energetic Materials, Southwest University of Science and Technology, Mianyang, Sicuan 621010, China*

[4]*Physics Department, School of Physics and Astronomy, Yunnan University, Kunming 650000, China*

(Received 10 March 2016; revised manuscript received 6 September 2016; published 10 March 2017)

We report the anisotropic magnetotransport measurement on a noncompound band semiconductor black phosphorus (BP) with magnetic field $\boldsymbol{B}$ up to 16 Tesla applied in both perpendicular and parallel to electric current $\boldsymbol{I}$ under hydrostatic pressures. The BP undergoes a topological Lifshitz transition from band semiconductor to a zero-gap Dirac semimetal state at a critical pressure P_c, characterized by a weak localization-weak antilocalization transition at low magnetic fields and the emergence of a nontrivial Berry phase of π detected by SdH magneto-oscillations in magnetoresistance curves. In the transition region, we observe a pressure-dependent negative MR only in the $\boldsymbol{B}\|\boldsymbol{I}$ configuration. This negative longitudinal MR is attributed to the Adler-Bell-Jackiw anomaly (topological $\boldsymbol{E}\cdot\boldsymbol{B}$ term) in the presence of weak antilocalization corrections.

DOI: 10.1103/PhysRevB.95.125417

I. INTRODUCTION

More recently a new kind of topological materials termed Dirac or Weyl semimetal, three-dimensional (3D) analogs of two-dimensional graphene, has been intensively investigated both theoretically and experimentally in that Dirac or Weyl semimetal is a phase of matter that provides a solid state realization of chiral Weyl fermions [1–8]. Most of its unique physics is a consequence of chiral anomaly, namely nonconservation of the number of quasiparticles of a given chirality. This extraordinary property is notably characterized by a large and strongly anisotropic negative magnetoresistance (MR) which exists in the case when the electric and magnetic fields are collinearly aligned. Indeed, following the theoretical prediction, the chiral anomaly-induced negative MR has been notably realized in Dirac semimetal Cd_3As_2 [9,10] and Na_3Bi [11], Weyl semimetal TaAs [12,13], $ZeTe_5$ [14], and noncentrosymmetric Weyl semimetals NbAs [15] and NbP [16]. However, a sizable negative MR also exist in semimetals which lack Dirac linear dispersion, such as $Cd_xHg_{1-x}Te$ [17], PdCoO [18], and half-Heusler GdPtBi [19]. The question naturally arises whether the chiral-related negative MR is an intrinsic property of Dirac or Weyl semimetal. Therefore, it is desirable to search for the origin of negative MR in a broader class of semimetals.

Recently the narrow band-gap semiconductor, black phosphorus (BP), has been revived owing to the realization of monolayered crystalline structure (phosphorene) and the exhibition of promising carrier mobilities, possible a new candidate for next-generation electronic and spintronic devices [20–24]. Fundamentally, BP has a relatively low band gap which can be further reduced by increasing the interlayer coupling. As its counterparts, slight change in the crystal structure thus strongly modifies the band gap of BP [25,26]. In particular, first-principle calculation predicts that BP possess a unique band structure, whose dispersion is nearly linear along the armchair direction [27,28]. Recent photoemission and magnetotransport measurements appear to support the theoretical prediction that bulk BP host the 3D Dirac semimetal phase [29,30]. Therefore, in such a Dirac semimetal of BP, there is strong interest in whether the chiral anomaly can be detected as a negative contribution to the longitudinal MR. In this paper we apply a moderate hydrostatic pressure to drive bulk BP into a semimetallic state. By anisotropic magnetoresistance measurements in this topological phase transition region we observe a large negative MR only in the presence of electric and magnetic fields aligned collinearly. This negative longitudinal MR is attributed to the Adler-Bell-Jackiw anomaly (topological $\boldsymbol{E}\cdot\boldsymbol{B}$ term) in the presence of weak antilocalization corrections.

II. EXPERIMENT

Black phosphorus crystal was prepared by the reaction of AuSn, red phosphorus, and SnI_4 in evacuated silica ampules. The starting stoichiometry followed Ref. [23]. The crystal structure was examined by x-ray diffraction, and only (001) peaks were observed with the full-width-at-half maximum around 0.1, as shown in Fig. 1, which indicates good crystallization of our samples.

Samples were pressurized in a PPMS-supported piston cylinder clamp cell made of Be-Cu alloy. The inner jacket of the cell was made of alloy NiCrAl and Daphne 7373 as the pressure transmission medium. A calibrated cernox thermometer was attached directly on the cell close to the samples to measure temperature. For each measurement run the pressure P inside the cell was determined by monitoring the magnitude change of critical transition temperature ΔT_c of a lead (Pb) film stripe (∼300 nm in thickness) in four-probe

*cong_ren@iphy.ac.cn
†gfchen@iphy.ac.cn

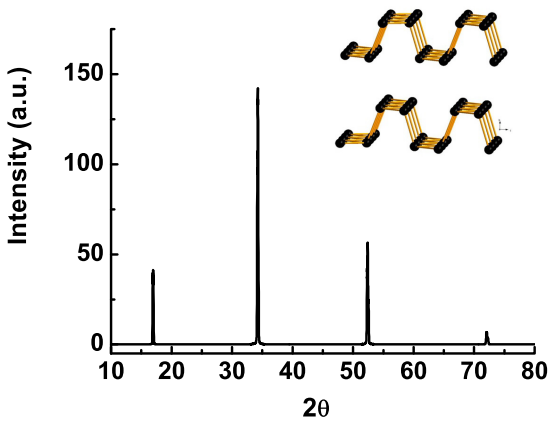

FIG. 1. X-ray diffraction pattern of the black phosphorene crystal. The right-up inset illustrates the atomic structure of BP (the perspective side view of few-layer phosphorene).

measurement. We also checked whether the pressure inside the cell relaxes by comparing the T_cs of Pb film before and after all the measurement. By this method the pressure inside the cell is about 2% in error limit.

III. RESULTS AND DISCUSSIONS

Figure 2(a) schematically illustrates the pressure dependence of band structures of bulk BP using first-principle electronic structure calculations. As calculated, the semiconducting system opens a gap of several hundred milli-eV at ambient pressure. With increasing pressure P, the semiconducting band gap gradually closes and the two bands below and above Fermi energy E_F touch at the Z point. The band inversion happens when further increasing P, and an inversion gap is reopened at crossing points due to finite spin-orbit coupling. Experimentally, the BP crystal is a p-type semiconductor with an activation energy of $E_g \simeq 8.6$ meV in resistivity ρ vs temperature (T) at ambient pressure, as shown in the inset of Fig. 1(b). Upon the applied P the resistive divergence at low Ts is gradually suppressed and a completely metallic state in the whole T range occurs as $P \geqslant 1.52$ GPa, as shown in the main panel of Fig. 2(b). This dramatic resistivity change with P-driven semiconductor-to-metal (STM) transition was also observed in 3D topological Kondo insulator SmB_6 near a quantum critical pressure of 5.4 GPa [31]. For a rough estimate of the critical pressure P_c for STM transition in our BP samples, we choose residue-resistance-ratio [$RRR \equiv R(300K)/R(2K)$] as a function of P, as shown in Fig. 2(c). In this scenario, the critical pressure for STM transition is between 0.8 and 1.1 GPa. Moreover, as shown in Fig. 1(c), RRR scales with P as $RRR \propto \exp(-aP)$ on the semiconducting side ($P < P_c$), implying a P-dependent band gap and eventually, a zero-gap semiconductor at P_c for BP. A similar result has been obtained in P-dependent ρ-T measurement [25].

To identify the nature of the P-induced STM transition and to provide useful information on Fermi surface topology for metallic BP, we performed magnetoresistance measurements with magnetic field B applied parallel ($B\|c$) and perpendicular ($B\|b$) to the basal c plane, respectively. It is noted that in

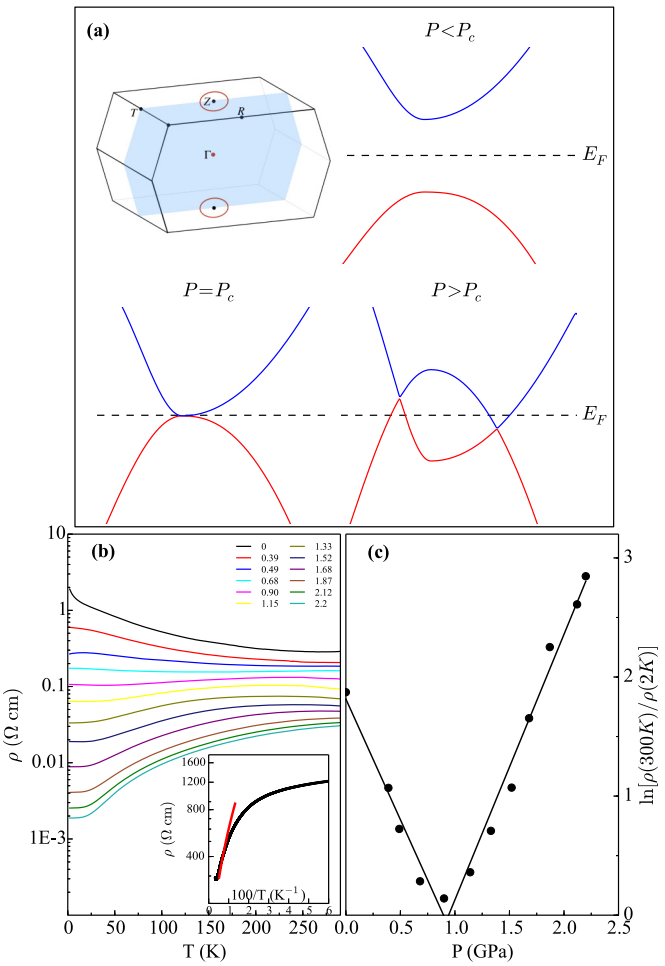

FIG. 2. (a) Brillouin zone and the evolution of the band structure diagram of the black phosphorus under hydrostatic pressures. Band structures are calculated by using the Vienna *ab initio* simulation package (VASP) based on generalized gradient approximation in Perdew-Burke-Ernzerhof (PBE) pseudopotential, the spin-orbit coupling (SOC) is included in our calculation. (b) Transverse resistivity ρ_{xx} as a function of temperature T under several hydrostatic pressures. Inset: The semilogarithmic plot of resistivity vs $1/T$ at ambient pressure. The red solid line is the linearly fitting line. (c) The semilogarithmic plot of residue-resistance-ratio [$RRR \equiv R(300K)/R(2K)$] as a function of P. The solid lines are linear fits in the limited pressure region, respectively.

parallel $B\|c$ the magnetic field is perpendicular to the current I, transverse magnetoresistance TMR. On the contrary, in perpendicular B is in the parallel direction of I, namely, $B\|I$ the so-called Lorentz-force-free configuration, resulting in the longitudinal magnetoresistance LMR. Figure 3 summarizes the main results of magnetoresistance (MR) measurement at varied Ps and Ts with $B\|c$ and $B\|b$, respectively. At $P \leqslant 0.9$ GPa in Figs. 3(a) and 3(b), the MR $\equiv \frac{\rho(B)-\rho(0)}{\rho(0)}$ data show a sharp peak (negative) MR at low fields for both $B\|c$ and $B\|b$. In this pressure region, the negative MR in the low field is attributed to weak localization (WL) effect in band semiconducting state [32–35]. However, as P approaches to $P_c = 1.14$ GPa, the negative MR completely vanishes, leaving a relatively sharp positive MR superimposed

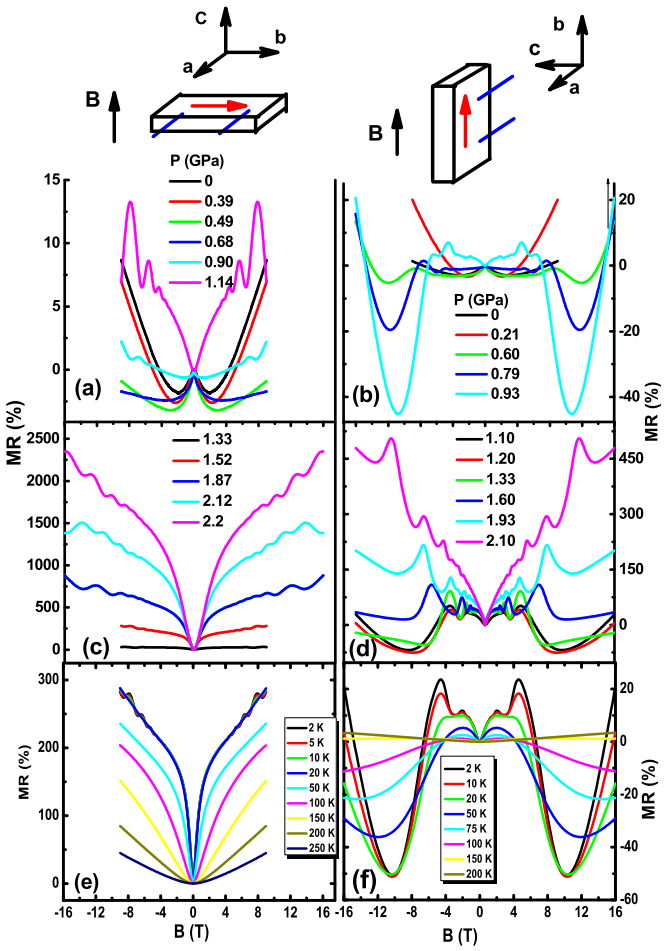

FIG. 3. (a) (c) Pressure dependence of magnetoresistance ($MR \equiv \frac{\rho(B)-\rho(0))}{\rho(0)}$) at $T = 2$ K with magnetic field B parallel to the c axis. (b) (d) Pressure dependence of magnetoresistance at $T = 2$ K with magnetic field B parallel to the b axis. The upper insets of (a) and (b) are schematic of the measurement configuration for $B\|c$ and $B\|b$, respectively. The red arrowed lines show the electric current with respect to the applied magnetic field. (e) Temperature dependence of MR with $B\|c$ under $P = 1.52$ GPa. (f) Temperature dependence of MR with $B\|b$ under $P = 1.20$ GPa.

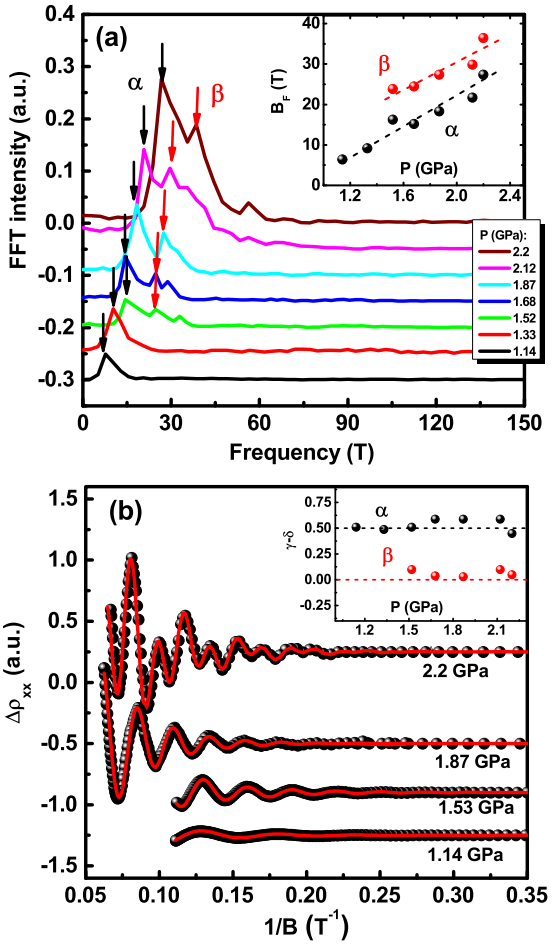

FIG. 4. (a) FFT spectrum of $-\mathrm{d}^2\rho_{xx}/\mathrm{d}B^2$ as a function of pressure at $T = 2$ K for $B//c$ configuration. The black- and red-arrowed lines trace the peaks of the FFT spectrum for different Fermi pockets α and β, respectively. The spectrum lines are vertically shifted for clarity. Inset: Pressure dependence of the FFT spectrum frequency for α and β pockets. The colored dash-lines are the guide lines in a linear form. (b) The SdH oscillations $\Delta\rho_{xx} = \rho_{xx} - \overline{\rho_{xx}}$ as a function of inverse magnetic field $1/B$ at $T = 2$ K under various pressures. The red solid lines are the fits to the data based on Eq. (1) for extracting the values of the phase $|\gamma - \delta|$ of α and β pockets. The data points and their fits are shifted for clarity. Inset: The extracted phase $|\gamma - \delta|$ as a function of pressure for α and β pockets.

on underlying magneto-oscillations for $P \geqslant P_c \simeq 1.14$ GPa, as clearly illustrated in Fig. 3(a). These dips in MR are similar to those observed in a thin film of magnetically doped Bi_2Se_3 topological insulators [34–36], graphene [37,38], and 3D Dirac semimetal Cd_3As_2 [39], which is a characteristic feature of weak antilocalization (WAL) effect [38].

Generally, WL-WAL transition at low magnetic field is a consequence of the emergence of topological band structure. The destructive interference due to the π Berry phase in momentum k space can give an enhancement to the classical electronic conductivity in small magnetic fields, leading to a peculiar weak antilocalization effect [37,38]. In addition, the emergence of a nontrivial Berry phase at $P > P_c$ has been confirmed by analyzing the magneto-oscillations imposing on the MR curves at high magnetic fields.

Studies of Shbonikov-de Haas (SdH) oscillations in magnetoresistance provide a unique opportunity to gain insight into the nature of the Fermi surface topology including the P-induced semimetal states in BP. As displayed in Figs. 3(a) and 3(b), a large SdH quantum oscillation can be resolved in MR curves even at $P \sim 0.9$ GPa before in semimetal states ($P \geqslant P_c$). Typically, to better resolve the SdH oscillations, we take the second derivative of resistivity $-d^2\rho_{xx}/dB^2$ as a function of inverse magnetic field $1/B$. By performing a fast Fourier transformation (FFT) on such $-d^2\rho_{xx}/dB^2$, we derived oscillation frequencies B_F shown in the main panel of Fig. 4(a). As shown from the FFT spectrum, while a band is labeled α pocket with a lower frequency B_F is present in the whole pressure region. A band of β pocket manifests itself as a second peak in the FFT spectrum at $P > 1.68$ GPa with a higher frequency. In the inset of Fig. 4(a), we show the oscillation frequency B_F as a function of P for both the α and

β bands. It is noted that the β band can only be resolved in our MR measurement at $P \geqslant 1.52$ GPa.

A consequence of the combination of time-reversal symmetry with the novel Dirac point structure can be viewed in terms of Berry's phase arising from the band degeneracy point. For a three-dimension electron system, a direct probe of such Berry's phase in the magnetic field regime is simply based on a semiclassical magneto-oscillation description:

$$\rho_{xx} = \overline{\rho_{xx}} \left\{ 1 + \sum_{i=\alpha,\beta} A_i(B,T) \cos[2\pi(B_{Fi}/B + \gamma_i - \delta)] \right\}. \tag{1}$$

Here $\overline{\rho_{xx}}$ is the nonoscillatory part of the resistivity, $A(B,T)$ is the SdH oscillation amplitude, and the offset δ is a phase shift determined by the dimensionality [40]. In this formula, the Onsager phase γ is related to the Berry's phase ϕ_B by $\gamma = |1/2 - \phi_B/2\pi|$. In a topologically trivial band with a parabolic dispersion, the Berry's phase $\phi_B = 0$ and equivalently $\gamma = 1/2$, whereas, in a Dirac electronic system with a linear band dispersion, $\gamma = 0$ due to a topologically nontrivial Berry's phase $\phi_B = \pi$. Experimentally, the value ϕ_B or equivalently γ can be determined through the plot of Landau level (LL) fan diagram in SdH oscillation effects in MR. However, for an electronic system composed of multiple bands, the plot of the LL fan diagram of SdH oscillation pattern is no longer a reliable method to extract the Berry's phase [41]. Alternately, we analyze the SdH oscillation by performing nonoscillatory subtraction and fitting the resulted oscillating $\Delta\rho_{xx}$ using the obtained FFT frequencies B_Fs in Eq. (1). The two band fitting yields the values of $\gamma - \delta$ for α, β bands as fitting parameter, shown in the inset of Fig. 4(b). Due to the smaller carrier density and π Berry phase, by comparison with first-principle calculations it is more likely that the β pocket is Dirac fermions with nontrivial Fermi surface topology, whereas the α pocket is holelike with a trivial Berry's phase in momentum space.

Intriguingly, the appearance of strong magneto-oscillations *at high magnetic fields* at such P_c and the WL-WAL crossover *at low fields* are accompanied with a dramatic enhancement of the MR ratio, reaching a large value of ~2200% at 16 T with no indication of MR saturation, as shown in Fig. 3(c). Similar large positive MR for $B \| c$ has been reported in a number of semimetals, such as WTe_2 [42], TaAs [12,13], and bismuth [43], and has been attributed to the electron-hole compensation effect. Very recently, a titanic nonsaturating MR of 80 000% in a more insulating BP sample has been observed and coincident with a sign reversal of Hall effect from negative (electron-type) to positive (hole-type) transition at $P_c \simeq 1.2$ GPa [30]. Combining with all of these experimental observations, including a P-dependent zero-band gap state, the WL-WAL crossover and the emergence of an electron pocket with nontrivial Berry phase points to a topological phase transition of the BP band structure at P_c.

In Figs. 2(b) and 2(d), a distinguishing feature is that in longitudinal MR curves with $B \| I$, a large negative MR appears at relatively high fields between 4 T and 8 T in the pressure region of $0.6 \sim 1.6$ GPa. Under higher P, the negative LMR disappears even in a Dirac semimetal state, restoring to a normally quadratic MR with Landau oscillation level. It can be seen that the negative LMR is beside on the WAL, reaching a maximum value of −60% before an upturn to positive LMR at higher magnetic fields at $P = 1.2$ GPa. To clearly observe the negative LMR, we increase Ts to suppress the magneto-oscillations in MR. As shown in Fig. 3(f), below 20 K, the level of the negative LMR is nearly T independent. With increasing T, both the negative LMR and the WAL effect are suppressed, and ultimately disappear above 150 K. In contrast, shown in Figs. 2(c) and 2(e), the TMR curves show fully positive values in semimetal state ($P \geqslant P_c$), even no tendency toward a negative MR both in Ps and in Ts. To double check the occurrence of the negative MR only in the parallel configuration, we also measured the MR curves with $B \| a$ axis up to 16 T and the electric current always in the ab plane under the same pressures (not shown here). In these transverse MR curves, no trace of negative MR is found.

From the MR point of view, the appearance of negative LMR is rare for nonferromagnetic systems due to the absence of Lorentz force acting on the electron/quasiparticle system. However, for topological materials it is believed that negative LMR is a signature of the chiral anomaly, i.e., nonconservation of the chiral charge in the present of collinear-oriented E and B. Burkov [44] argued that the occurrence of chiral anomaly-driven negative LMR has two crucial ingredients. One is the magnetic field-induced coupling between the chiral and the total charge densities. This arises from the Berry curvature and is present in principle whenever the Berry curvature is nonzero. In this case the observation of negative LMR is nonspecific to Dirac and Weyl metals. However, only when the chiral charge density is a nearly conserved quantity, the coupling between the chiral and the total charge densities leads to a large negative LMR. This property is specific to Dirac and Weyl metals and is realized only when the Fermi energy is close to Weyl nodes.

To demonstrate the chirality-related nature of the negative LMR of BP, we show in Fig. 5(a) the LMR curves under various Ps at an elevated $T = 50$ K. As shown, the negative LMR is strongly P dependent in magnitude. At $P < P_c$, the level of the negative LMR increases with P, as arrow marked in Fig. 5(a). At $P_c = 1.12$ GPa, the negative LMR reaches a maximum of −40% in magnitude, and then it decreases and completely disappears, entering a positive LMR state at $P > 1.33$ GPa. Figure 5(b) shows the linear dependence of the magnitude of negative LMR on P. This behavior of the negative LMR is similar to the topological phase transition based on RRR criterion [Fig. 2(c)], indicative of the touching/closing of the band gap reaching a generic Weyl node point at E_F in the band structure of 3D Dirac semimetals. This Weyl node-related negative LMR is the most prominent signature in magnetotransport for the chiral anomaly for BP.

For a quantitative estimate of the chiral anomaly-induced negative LMR, we attribute the underlying mechanism for the negative MR to the Adler-Bell-Jackiw (ABJ) anomaly in the presence of WAL corrections. Based on a semiclassical theory of motion for the momentum, Kim *et al.* developed the equation describing the ABJ anomaly and possible scattering channels of motion for the momentum [36,45]. In their model, the longitudinal magnetoconductivity (MC) in the weak field region is expressed as:

$$\sigma_L(B) = (1 + C_W B^2) \cdot \sigma_{WAL} + \sigma_n, \tag{2}$$

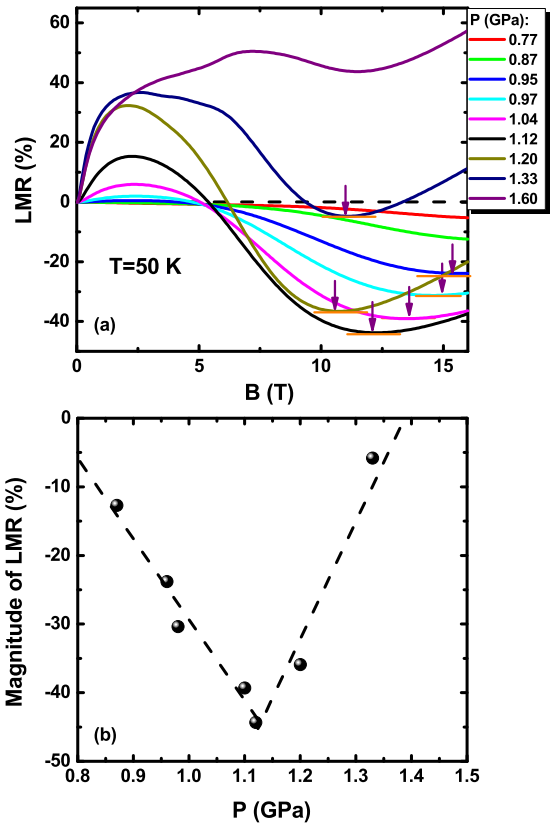

FIG. 5. (a) Pressure dependence of MR in the parallel configuration ($B\|b$). The arrows mark the trace of the turning points in such LMR curves (the minimum level of the LMR). (b) The magnitude of negative MR as a function of applied pressure at $T = 50$ K. The dashed lines are linear fits in the limited pressure region, respectively.

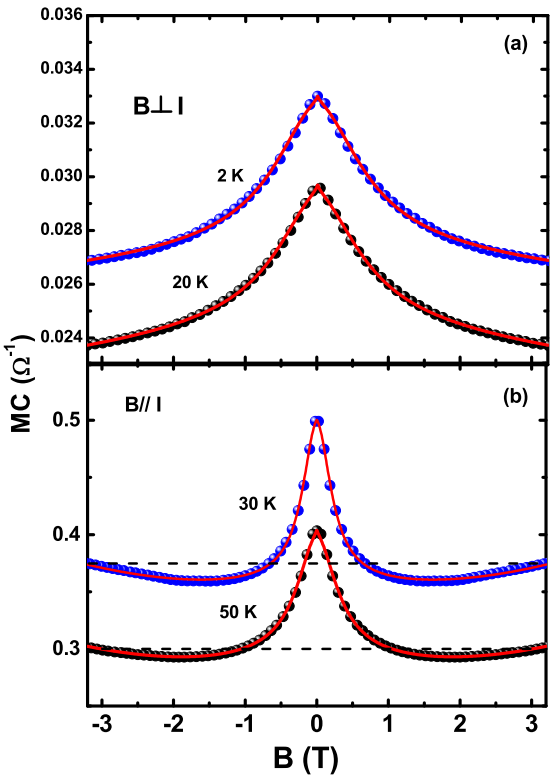

FIG. 6. (a) Magnetoresistance in the form of magnetoconductance (MC) $\delta\sigma_{xx} \equiv \sigma_x(B) - \sigma_{xx}(0) \simeq -MR/\rho_{(0)}^2$ under $P = 1.33$ GPa. The red solid lines are the theoretical fits for different Ts, see in text. (b) Magnetoconductance MC under $P = 1.35$ GPa for selected Ts in $B\|b$ configuration. The colored solid lines are the theoretical fits to Eq. (2) for different Ts.

with σ_{WAL} the conductivity from WAL corrections associated with scattering and σ_n being that from conventional Fermi surface contributions. Here the factor $C_W B^2$ with a positive constant C_W originates from the topological $(\mathbf{E}\cdot\mathbf{B})\Omega_b$ term in the equation (Ω_b the Berry curvature in momentum). It is noted that a $\sim B^2$ term of chiral magnetic effect for topological systems has been deduced theoretically by Son *et al.* [46] and Kharzeev *et al.* [47]. On the other hand, the transverse MC is expressed as $\sigma_T(B) = \sigma_{WAL} + \sigma_n$ without the anomaly contribution because of vanishing of the contribution from the $\mathbf{E}\cdot\mathbf{B}$ term. Figures 6(a) and 6(b) show the typical transverse MC and longitudinal MC curves at different Ts in the limited magnetic field region of $-4 < B < 4$ T, respectively, with their correspondingly theoretical fitting based on the above equations. As shown, the theoretical fits to the data reproduce quite well the essential features of these MC curves, yielding the important parameters as: $C_W = 1.39\times10^{-2}\ T^{-2}$ for $T = 30$ K and $C_W = 1.0\times10^{-2}\ T^{-2}$ for $T = 50$ K for the longitudinal MC curves. From these parameters, it can be sensed that with increasing T, the value of C_W decreases. As expected, C_W should be zero with a vanish of the downturn of the longitudinal MC at high Ts.

IV. CONCLUSIONS

In conclusion, we have performed bulk transport measurements on single crystals of black phosphorus under hydrostatic pressure. At a critical pressure of 0.9 ∼ 1.2 GPa, BP undergoes a semiconductor to metal transition with a large MR ratio as high as 2200%. By analyzing the Shubnikov-de Haas oscillations imposed on the MR, it yields a nontrivial Berry's phase as expected for the relativistic Dirac cone. When the magnetic field is parallel to the current, chiral anomaly induced negative MR up to −45% is observed, providing the experimental results on quantum transport of Dirac fermions in black phosphorus.

ACKNOWLEDGMENTS

C.R. wishes to express his thanks to Prof. J. R. Shi and Drs. Jun Zhu and X. C. Huang for valuable discussions. This study is supported by the National Science Foundation of China (Nos. 11574373, 11574372) and the Ministry of Science and Technology of China (973 project Nos: 2011CBA00100, 2015CB921303, and 2011CB821404), the National Key Research Program of China under Grant No. 2016YFA0300604, the 'Strategic Priorty Research Program (B)' of the Chinese Academy of Science under Grant No. XDB07020100, and Chinese Academy of Sciences (Project ITSNEM).

[1] H. B. Nielsen and M. Ninomiya, Phys. Lett. B **130**, 389 (1983).
[2] Chen Fang, Matthew J. Gilbert, Xi Dai, and B. Andrei Bernevig, Phys. Rev. Lett. **108**, 266802 (2012).
[3] S. Murakami, New J. Phys. **9**, 356 (2007).
[4] S. M. Young, S. Zaheer, J. C. Y. Teo, C. L. Kane, E. J. Mele, and A. M. Rappe, Phys. Rev. Lett. **108**, 140405 (2012).
[5] A. A. Burkov, M. D. Hook, and L. Balents, Phys. Rev. B **84**, 235126 (2011).
[6] Q. D. Gibson, L. M. Schoop, L. Muechler, L. S. Xie, M. Hirschberger, N. P. Ong, R. Car, and R. J. Cava, Phys. Rev. B **91**, 205128 (2015).
[7] Z. Wang, Y. Sun, X.-Q. Chen, C. Franchini, G. Xu, H. M. Weng, X. Dai, and Z. Fang, Phys. Rev. B **85**, 195320 (2012).
[8] Z. Wang, H. M. Weng, Q. Wu, X. Dai, and Z. Fang, Phys. Rev. B **88**, 125427 (2013).
[9] Z. K. Liu, B. Zhou, Z. J. Wang, H. M. Weng, D. Prabhakaran, S. K. Mo, Y. Zhang, Z. X. Shen, Z. Fang, X. Dai, Z. Hussain, and Y. L. Chen, Science **343**, 864 (2014).
[10] T. Liang, Quinn Gibson, Mazhar N. Ali, Minhao Liu, R. J. Cava, and N. P. Ong, Nat. Mater. **14**, 280 (2014).
[11] Jun Xiong, Satya K. Kushwaha, Tian Liang, Jason W. Krizan, Max Hirschberg, Wudi Wang, R. J. Cava, and N. P. Ong, Science **350**, 413 (2015).
[12] Xiaochun Huang, Lingxiao Zhao, Yujia Long, Peipei Wang, Dong Chen, Zhanhai Yang, Hui Liang, Mianqi Xue, Hongming Weng, Zhong Fang, Xi Dai, and Genfu Chen, Phys. Rev. X **5**, 031023 (2015).
[13] Cheng-Long Zhang, Su-Yang Xu, Ilya Belopolski, Zhujun Yuan, Ziquan Lin, Bingbing Tong, Guang Bian, Nasser Alidoust, Chi-Cheng Lee, Shin-Ming Huang, Tay-Rong Chang, Guoqing Chang, Chuang-Han Hsu, Horng-Tay Jeng, Madhab Neupane, Daniel S. Sanchez, Hao Zheng, Junfeng Wang, Hsin Lin, Chi Zhang, Hai-Zhou Lu, Shun-Qing Shen, Titus Neupert, M. Zahid Hasan, and Shuang Jia, Nat. Commun. **7**, 10735 (2016).
[14] Qiang Li, Dmitri E. Kharzeev, Cheng Zhang, Yuan Huang, I. Pletikosić, A. V. Fedorov, R. D. Zhong, J. A. Schneeloch, G. D. Gu, and T. Valla, Nat. Phys. **12**, 550 (2016).
[15] Xiaojun Yang, Yupeng Li, Zhen Wang, Yi Zheng, and Zhu-an Xu, arXiv:1506.03190.
[16] Chandra Shekhar, Ajaya K. Nayak, Yan Sun, Marcus Schmidt, Michael Nicklas, Inge Leermakers, Uli Zeitler, Zhongkai Liu, Yulin Chen, Walter Schnelle, Juri Grin, Claudia Felser, and Binghai Yan, Nat. Phys. **11**, 645 (2015).
[17] I. M. Tsidilkovskii, W. Giriat, G. I. Khans, and E. A. Neifeld, Status Solidi B **64**, 717 (1974).
[18] N. Kikugawa, P. Goswami, A. Kiswandhi, E. S. Choi, D. Graf, R. E. Baumbach, J. S. Brooks, K. Sugii, Y. Iida, M. Nishio, S. Uji, T. Terashima, P. M. C. Rourke, N. E. Hussey, H. Takatsu, S. Yonezawa, Y. Maeno, and L. Balicas, Nat. Commun. **7**, 10903 (2016).
[19] Max Hirschberg, Satya Kushwaha, Zhijun Wang, Quinn Gibson, Carina A. Belvin, B. A. Bernevig, R. J. Cava, and N. P. Ong, Nat. Mater. **15**, 1161 (2016).
[20] H. Liu, A. T. Neal, Z. Zhu, Z. Luo, X.-F. Xu, D. Tomanek, and P. D. Ye, ACS Nano **8**, 4033 (2014).
[21] Andres Castellanos-Gomez, J. Phys. Chem. Lett. **6**, 4280 (2015).
[22] Likai Li, Fangyuan Yang, Guo Jun Ye, Zuocheng Zhang, Zengwei Zhu, Wenkai Lou, Xiaoying Zhou, Liang Li, Kenji Watanabe, Takashi Taniguchi, Kai Chang, Yayu Wang, Xian Hui Chen, and Yuanbo Zhang, Nat. Nanotech. **11**, 593 (2016).
[23] Xi Ling, Han Wang, Shengxi Huang, Fengnian Xia, and Mildred S. Dresselhaus, Proc. Natl. Acad. Sci. USA **112**, 4523 (2015).
[24] G. Long, S. G. Xu, Z. F. Wu, T. Y. Han, J. X. Z. Lin, J. Y. Shen, Y. Han, W. K. Wong, J. Q. Hou, R. Lortz, and N. Wang, Nano Lett. **16**, 7768 (2016).
[25] A. Morita, Appl. Phys. A **39**, 227 (1986).
[26] M. Okajima, S. Endo, Y. Akahama, and S. Narita, Jpn. J. Appl. Phys. **23**, 15 (1984).
[27] R. X. Fei, Vy Tran, and Li Yang, Phys. Rev. B **91**, 195319 (2015).
[28] J. Z. Zhao, R. Yu, H. M. Weng, and Z. Fang, Phys. Rev. B **94**, 195104 (2016).
[29] J. Kim, S. S. Baik, S. H. Ryu, Y. S. Sohn, S. Park, B.-G. Park, J. Denlinger, Y. Yi, H. J. Choi, and K. S. Kim, Science **349**, 723 (2015).
[30] Z. J. Xiang, G. J. Ye, C. Shang, B. Lei, N. Z. Wang, K. S. Yang, D. Y. Liu, F. B. Meng, X. G. Luo, L. J. Zou, Z. Sun, Y. B. Zhang, and X. H. Chen, Phys. Rev. Lett. **115**, 186403 (2015).
[31] S. Gabáni, E. Bauer, S. Berger, K. Flachbart, Y. Paderno, C. Paul, V. Pavlík, and N. Shitsevalova, Phys. Rev. B **67**, 172406 (2003).
[32] Gerd Bergmann, Phys. Rep. **107**, 1 (1984).
[33] E. McCann, K. Kechedzhi, Vladimir I. Fal'ko, H. Suzuura, T. Ando, and B. L. Altshuler, Phys. Rev. Lett. **97**, 146805 (2006).
[34] Minhao Liu, Jinsong Zhang, Cui-Zu Chang, Zuocheng Zhang, Xiao Feng, Kang Li, Ke He, Li-li Wang, Xi Chen, Xi Dai, Zhong Fang, Qi-Kun Xue, Xucun Ma, and Yayu Wang, Phys. Rev. Lett. **108**, 036805 (2012).
[35] Huichao Wang, Haiwen Liu, Cui-Zu Chang, Huakun Zuo, Yanfei Zhao, Yi Sun, Zhengcai Xia, Ke He, Xucun Ma, X. C. Xie, Qi-Kun Xue, and Jian Wang, Sci. Rep. **4**, 5817 (2014).
[36] Heon-Jung Kim, Ki-Seok Kim, J.-F. Wang, M. Sasaki, N. Satoh, A. Ohnishi, M. Kitaura, M. Yang, and L. Li, Phys. Rev. Lett. **111**, 246603 (2013).
[37] F. V. Tikhonenko, A. A. Kozikov, A. K. Savchenko, and R. V. Gorbachev, Phys. Rev. Lett. **103**, 226801 (2009).
[38] Xiaosong Wu, Xuebin Li, Zhimin Song, Claire Berger, and Walt A. de Heer, Phys. Rev. Lett. **98**, 136801 (2007).
[39] Bo Zhao, Peihong Cheng, Haiyang Pan, Shuai Zhang, Baigeng Wang, Guanghou Wang, Faxian Xiu, and Fengqi Song, Sci. Rep. **6**, 22377 (2016).
[40] Shoenberg, *Magneto-Oscillation in Metals* (Cambridge University Press, Cambridge, 1984).
[41] A. A. Taskin and Yoichi Ando, Phys. Rev. B **84**, 035301 (2011).
[42] Mazhar N. Ali, Jun Xiong, Steven Flynn, Jing Tao, Quinn D. Gibson, Leslie M. Schoop, Tian Liang, Neel Haldolaarachchige, Max Hirschberger, N. P. Ong, and R. J. Cava, Nature (London) **514**, 205 (2014).
[43] Xu Du, Shan-Wen, D. L. Maslov, and A. F. Hebard, Phys. Rev. Lett. **94**, 166601 (2005).
[44] A. A. Burkov, Phys. Rev. B **91**, 245157 (2015).
[45] Yong-Soo Jho and Ki-Seok Kim, Phys. Rev. B **87**, 205133 (2013).
[46] D. T. Son and B. Z. Spivak, Phys. Rev. B **88**, 104412 (2013).
[47] K. Fukushima, D. E. Kharzeev, and H. J. Warringa, Phys. Rev. D **78**, 074033 (2008).